applied optics

Low-order aberration correction of the TMT tertiary mirror prototype based on a warping harness

Linchu Han,[1,*] Chengzhi Liu,[1] Cunbo Fan,[1] Zhenwei Li,[1] Jingxu Zhang,[2] and Xiaolin Yin[2]

[1]Changchun Observatory, National Astronomical Observatories, CAS, Changchun 130117, China
[2]Changchun Institute of Optics, Fine Mechanics and Physics, Chinese Academy of Sciences, Changchun 130033, China
*Corresponding author: hanlinchu1217@163.com

Received 4 December 2017; revised 29 January 2018; accepted 29 January 2018; posted 30 January 2018 (Doc. ID 314943); published 28 February 2018

A warping harness is proposed to simply and efficiently correct low-order aberrations that occur during manufacturing and operation of a telescope. For the Thirty Meter Telescope (TMT) tertiary mirror, the issue to be solved by the warping harness is particularly challenging due to its complicated load conditions and limited mounting space. In this study, first, a new type of whiffletree-based warping harness configuration applied to a ¼-prototype TMT tertiary mirror is presented and optimized using finite element analysis (FEA) to improve the output precision of the moment actuator. Next, based on the new configuration, a simulation method for a correction process is proposed. The results show that the root mean square value of the mirror-surface error converged from 64.9 to 25.4 nm after correction, which satisfied the requirement document of TMT. Finally, combined with the analysis and calculation results, the moment actuator testing system with high-precision displacement–force–strain is established to assess the system errors. The tests of the moment actuator displacement, stress, strain-output precision, linearity, and repeatability are completed, and all errors were found to be within a controllable range. The results show the validity and feasibility of the designed warping harness, which can prove its applicability in more complicated conditions and, to a certain degree, broaden the application scope of the warping harness.

OCIS codes: (090.1000) Aberration compensation; (220.0220) Optical design and fabrication; (230.4040) Mirrors; (120.6650) Surface measurements, figure.

https://doi.org/10.1364/AO.57.001662

1. INTRODUCTION

In a large-aperture ground-based telescope system, low-order aberrations, which are primarily induced by manufacturing error, gravity deformation, and temperature change, can directly affect the observation results. In addition, the reduced thickness of the mirror poses another challenge for the traditional passive support. When the mirror is thinner, the mirror surface error is more sensitive to the support structure, which leads to more obvious low-order aberrations. On the contrary, for active optics, the reduced thickness is a great advantage to correct the low-order aberrations. Therefore, to maintain the desired mirror surface during observation, a support structure with a high-precision correction system is essential.

During the development of low-order aberrations correction, active optics has made great progress [1,2]. However, for low-order aberrations caused by fabrication and assembly errors in large–thin mirrors, the active optics does not work as desired for the limited spatial correction frequency. To solve this problem, a new theory between passive and active optical supports, which is called semi-active optics [3], was proposed. It is mainly applied to large–thin mirrors and used at nearly zero bandwidth to correct low-order errors by providing warping to the mirror. As a new method of correcting low-order aberrations in semi-active optics, a warping harness was proposed to redistribute the three-point support forces by exerting momentum on the whiffletree pivots when a mirror surface cannot satisfy the requirements of low-order surface error. The schematic of the working principle of a warping harness is shown in Fig. 1. It should be noted that the whiffletree and the stepping motor are mounted on a mirror cell. Besides, the side of the mirror is also fixed on the mirror cell through the lateral support.

The warping harness evolves using the stress-polishing technology. It was used by Bernard Schmidt in making an axisymmetric correcting lens for a Schmidt telescope [4]. The theory and method for this technique are described by Everhart [5]. Nelson successfully processed an off-axis parabolic mirror using this technique. Then, a related idea was proposed by Leonard

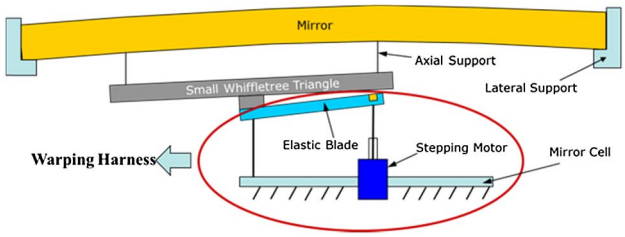

Fig. 1. Schematic of the working principle of the warping harness.

and Alvarez, which could adjust for astigmatism by bending a given mirror into another shape [6]. The earliest application was used in the Keck telescope. A set of leaf springs was manually adjusted to maintain the position of the segment, and the surface error improved from 110 nm root mean square (RMS) to 19 nm RMS [7,8]. This function was officially named "warping harness."

The support design for segments of the Thirty Meter Telescope (TMT) and the primary mirror in the European extremely large telescope (E-ELT) also adopted a similar structure [9]. However, for the TMT tertiary mirror, the issue to be solved by the warping harness is more challenging. First, the mounting space in the mirror cell for the warping harness is limited. However, to obtain a higher correction precision and simultaneously reduce the performance requirement of the actuator, generally a long elastic blade (or long force arm) is needed, which is in contradiction with the limited space. Therefore, the configuration should be specially designed. Besides, the tertiary mirror will be responsible for all the extra pointing, slewing, tracking, and guiding operations, which means that its load conditions are more complicated (sometimes even at almost 90° off the zenith). Under this condition, the surface error is very sensitive to the force of the support structure. As for the warping harness correction method, a higher output precision is demanded to meet the design requirements.

In the current study, considering limited space and the extremely strict mirror-surface precision demand, first, the structure of the warping harness applied to a ¼-prototype TMT tertiary mirror was designed and analyzed. Simultaneously, the warping harness configuration was optimized using FEA to improve the output precision of the moment actuator. Next, by using the Zernike polynomial fitting method, the best correction moment combination introduced by the warping harness, which can minimize the RMS value of the mirror surface, was simulated, and the correction results were obtained. Finally, according to the analysis and calculation results, the system error of the moment actuator was provided, and a testing system with high-precision displacement–force–strain was established to verify the output accuracy. The experimental results show the validity and feasibility of the designed warping harness and its correction ability.

2. STRUCTURE DESIGN AND ANALYSIS

The active correction of the warping harness is based on an 18 point whiffletree of the ¼-prototype TMT tertiary mirror [10,11]. The prototype TMT tertiary mirror is a flat oval mirror with a size of 898.5 mm × 634 mm and a thickness of 12.5 mm [12]. The warping harness can possibly change the load distribution in the flexible rod and cause a change in the surface figure by introducing discrete moments at the whiffletree joints. The key technology of the warping harness component design includes three contents: structure design, fitting of the mirror surface, and calculation of the corrected moments.

A. Structure Design of the Warping Harness Component

Implementing the experience gained from the warping harness design of Keck and TMT, the warping harness for the prototype TMT tertiary mirror also adopts elastic blades combined with a stepping-motor-driven configuration. The structure design of the warping harness mainly includes two parts: elastic-blade and actuator designs. The structure schematic diagram is shown in Fig. 2.

The elastic blade actually functions to generate elastic deformation using the actuator output displacement, which can produce a coupling moment at the center of the blade. Each elastic blade is fixed to a tripod by bolts. The actuator is composed from top to bottom of the drive nuts, transmission rod, connecting device, oil-free bushings, flexible-shaft coupling, and stepping motor.

1. Design and Analysis of the Elastic Blade

The elastic blade must be sufficiently flexible to ensure that the actuator stroke meets the requirements, which means that if the elastic blade is hard, and the calculated actuator force is very small, the stepping motor cannot achieve the accuracy even with the shift in its extremity. Therefore, the design of the elastic blade has mainly two functions: to generate deformation as the force arm and to increase the working stroke as far as possible using a certain force provided by actuator, which can improve the precision of the force output.

By considering the material properties, we select magnalium because it is a powerful alloy with better mechanical properties, as listed in detail in Table 1.

In accordance with the blade size, the warping harness outputs moments from the stepping motor that act on the whiffletree pivot. Furthermore, the flexibility of the warping harness can significantly affect the precision of the output moment. The flexibility of the blades must be compatible with the output moment so that the motor displacement can produce

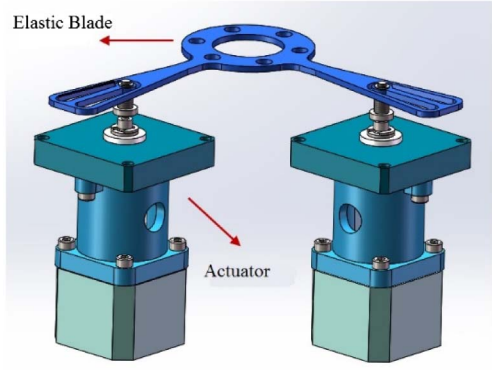

Fig. 2. Structure schematic of the warping harness.

Table 1. Elastic-Blade Material Properties

Young's Modulus	71,000 MPa
Density	2.81×10^{-6} kg/mm^3
Expansion coefficient	23.6×10^{-6}/°C
Poisson's ratio	0.33
Ultimate tensile strength	572 MPa
Ultimate yield strength	503 MPa
Hardness	150
Elongation	11

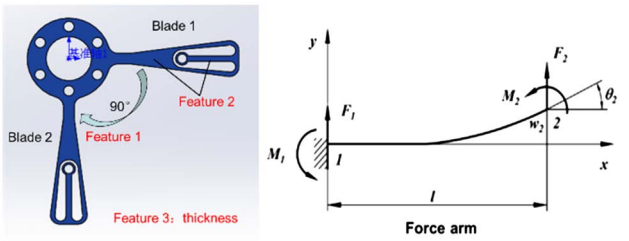

Fig. 3. Structure design and stress analysis of the elastic blade. Feature 1 is the two orthogonal blades; Feature 2 is the secondary moment transmission; Feature 3 is the optimized thickness of the blade.

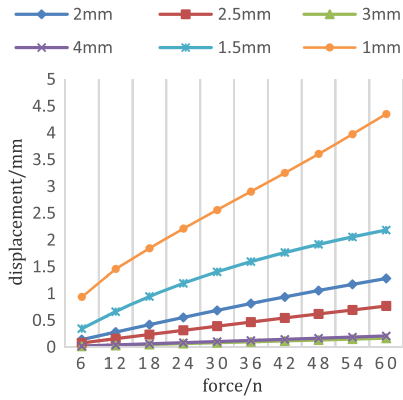

Fig. 4. Analysis of nonlinearity caused by geometric size of the blade.

Table 2. Warping Harness Blade Size

Length (Function Points Away from the Center Hole)	60 mm
Thickness	2 mm
External/Internal diameter	22/12.3 mm

reasonable strokes, and the output precision can be controlled. The structure design and stress analysis of the elastic blade are shown in Fig. 3.

Six threaded holes are located at the center of the blade, which are used to fix the tripod of the whiffletree. The blade configuration is a key design decision in the new type of warping harness. The features can be summarized in three aspects: first, two blades of the elastic blade are perpendicular to each other, which is aimed to guarantee that the coupling force provided by the elastic deformation acting on the tripod can maintain consistency at the center of the hole irrespective of the direction; second, owing to the limited mounting space in the mirror cell, a structure of secondary moment transmission for each blade is adopted to increase the length of force arm of the warping harness. By this means, a higher correction precision and smaller mounting space can be guaranteed simultaneously. Last but not least, the thickness of the elastic blade should be optimized to make it have a reasonable flexibility. On the one hand, a large stroke along the axial direction of the actuator can improve the correction resolution or precision. On the other hand, the output displacement of the actuator is required to be linear with the change of force. Based on the above two requirements, the thickness of the elastic blade is finally determined.

This study selects blades with thicknesses of 1, 1.5, 2, 2.5, 3, and 4 mm as objects. These blades are determined using the Workbench Static Analysis module. We introduce equal forces to act on the blades with varying thickness. A nonlinear analysis of the axial displacement is conducted to determine how the value changes with time. The analysis results are shown in Fig. 4. We can see that the curves of the 1- and 1.5-mm-thick blades are characterized by nonlinearity, whereas those of the 2-mm-thick and thicker blades are characterized as linear with no obvious difference. The thinner the elastic blade is the larger the stroke of the actuator output displacement is. On the one hand, a large stroke can improve the precision of the actuator output. On the other hand, we infer that the displacement of the elastic blade with time is linear. Thus, the 2 mm thickness is eventually selected, and the warping harness configuration is confirmed, as listed in Table 2.

The elastic blade generates elastic deformation because of the repeatedly applied stepping motor output force, which can be considered as mechanical fatigue. The fatigue life of the structure is determined by the continuous and repetitive application of the load. The effect factors on the fatigue life mainly include tension, compression, bending force, and torque. The elastic blade of the warping harness mainly bears a bending force. Because an observation station is used for approximately 50 years, the design of the system and its component for the telescope must continuously work for more than 50 years. The TMT is demanded to work for 10 h every night as a scientific observation time with effectiveness of 97%. We estimate that the elastic blades of the warping harness will correct the mirror five times per hour. Hence, the fatigue life of the elastic blade will amount to more than 8.85×10^5 times. Because the elastic blade is a part of the mirror-surface correction, it bears the changes in the stress after repeated elastic deformation, and the position of the root of the blade suffers the biggest stress. Thus, the blade-fatigue analysis is necessary. The smallest position of the cross-sectional area is also the maximal flexibility position, in which its weakness leads to stress concentration. The stress concentration extent of the weakness is denoted by K_T. Fatigue–stress concentration factor K_f can be expressed as

$$K_f = 1 + \frac{K_T - 1}{1 + a/\rho}, \tag{1}$$

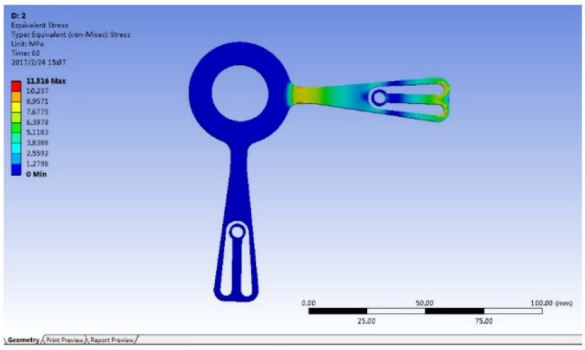

Fig. 5. Stress analysis of the elastic blade.

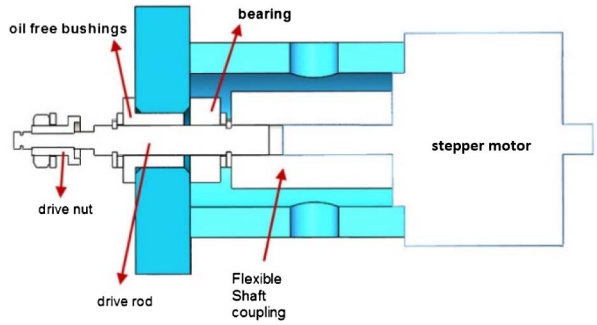

Fig. 6. Actuator schematic of the warping harness.

where ρ is the radius of the weak root, and a is the structural material constant. We assume the use of stress-field intensity of a weak area of fatigue to reflect the fatigue level, which can be expressed as

$$\sigma_F = \frac{1}{V}\int_{\Omega} f(\sigma_{ij})\varphi(r)\mathrm{d}v, \tag{2}$$

where Ω is the notch failure zone, V is the volume of the notch failure, $f(\sigma_{ij})$ is the notch failure stress function, and $\phi(r)$ is the weight function.

The elastic-blade material is aluminum alloy 7075 with Young's modulus $E = 71,700$ Mpa. The tensile strength is 572 Mpa. The elastic blade is subjected to cyclic loading of ± 1 N. According to the FEA, the maximum stress of the most vulnerable part of the elastic blade is 11.516 Mpa, as shown in Fig. 5. According to Eq. (2), the value of the weight function is one, and the calculated σ_F is 9.18 Mpa. Then, we use the S–N curve to obtain the fatigue life, which is 1.57×10^6.

2. Design of the Force Actuator

The force actuator is another part of the warping harness except for the elastic blade, which is the actuating mechanism of the correction system. The force actuator outputs displacement, and the displacement determines the value of the moment.

The commonly used force actuator structures are the following: motor lever type, screw type, and pneumatic hydraulic [13]. The motor lever type must consider the effect of the counter weight on the system, especially the error problem caused by friction between the lever and the structure of the pneumatic hydraulic. The control is relatively complex and needs to consider the possibility of air and liquid leakages. The screw type has a simple structure, which mainly considers the shaft stiffness. It is most often used in an active optical or electrical screw-type thin mirror. The warping harness actuator mainly provides the axial force of the structure to be as simple as possible, and the system stiffness requirement is relatively loose and considers the final design that uses the motor lead screw-type actuator.

The actuator structure includes a stepping motor, reducer, coupling, screw nut, and guide device. The application of a warping harness actuator in telescopes can be divided into two types. The first is the motor output linear displacement, which is converted to a moment by the blades acting on the whiffletree pivot. The second is the motor output angular displacement using a torsional spring converted to a moment.

Table 3. Technical Indicator of Stepping Motor

Name	Technical Indicator
Output force (N)	−1
Output accuracy (N)	0.01
Stroke (mm)	−3

According to the characteristics of the experimental platform and available space in the support system, we select an actuator in a blade form of a linear stepping motor. Figure 6 shows the schematic section diagram of the actuator, which includes a stepping motor, reducer, coupling, screw nut, and guide device.

Particularly, we need to select the stepping motor. The selection of stepper motor mainly considers three factors: step angle, static torque, and electricity. The step angle depends on the accuracy of the actuator output force, and the minimum resolution of the actuator output force converts to the rotation angle of the drive shaft, so the step angle should be less than or equal to the angle. Based on FEA, actuator output 0.01 N means the displacement output of the actuator is 0.0015 mm, which is equal to the stepping motor rotating 1.54°. It indicates that the stepper motor can realize that the minimum step angle is 1.54°. The actuator schematic diagram of the warping harness is shown in Table 3.

Finally, according to the previous step, the actuator specifications depend on the correction forces. An HSTM35 linear stepping motor is used, owing to its small volume and simple structure with a 1.8° step angle, holding torque of 75 N · mm, coil current of 1.0 A, height of 28 mm, width of 35 mm, 5 mm diameter shaft, and mass of 220 g.

Figure 7 shows the support system of the TMT tertiary mirror with a warping harness. Each actuator delivers a force to the elastic blade, resulting in the blade deformation. The blade center hole and tripod form a fixed connection. A correction force can be applied by deforming the blade so that it plays a direct role in the redistribution of the flexible-rod supporting force of the mirror, which is used to minimize the surface errors.

B. Analysis and Corrected Moment Calculation of the Warping Harness Component

Assuming that the support structure and the mirror will not produce interference, the distribution of the warping harness

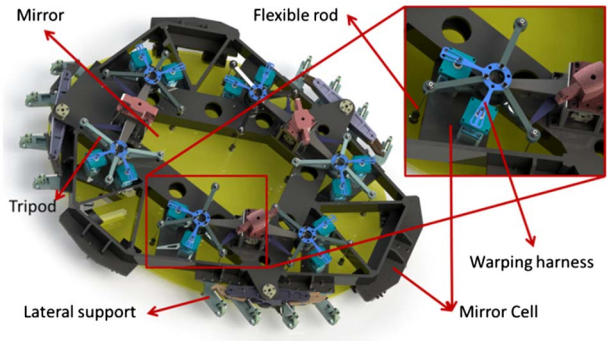

Fig. 7. Support system of TMT tertiary mirror with the warping harness.

in the TMT tertiary mirror support system is shown in Fig. 8. A pair of moment actuators (orthogonal to each other) is placed on each whiffletree pivot across each joint. The small dots indicate the position of the flexible support points, the large dots indicate the position of the tripod center hole, and the double arrows indicate the warping harness orientation. The 12 moment actuators are numbered in sequence from top to bottom and from left to right. Conditions 1–12, respectively, indicate that actuators 1–12 are influenced by a unit-corrected force, whereas condition 13 indicates a response to the gravitational effects on the axial orientation.

The response function of the mirror is based on the FEA method, which establishes a finite element model, and the modeling of each deformation is caused by the force actuator as a response function of the mirror.

After correction by the warping harness, the mirror surface is equal to the sum of the initial surface error plus each of the actuator influence functions scaled by the respective input of each actuator. $x_1 \sim x_{12}$ are the values of twelve correction forces. When the direction of gravity is parallel to the optical axis of the tertiary mirror, the deformation is selected as the initial mirror surface. The correction process can be described as shown in Fig. 9, where actuator 1 to actuator 12 are the surface deformations induced by 1 N force, respectively. The process also can be mathematically expressed as Eq. (3):

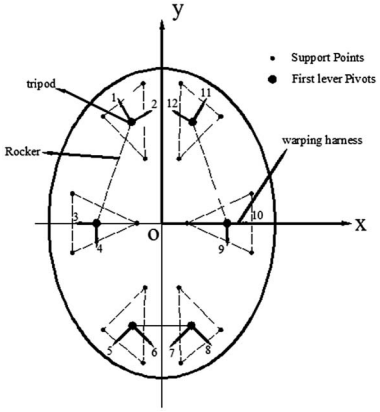

Fig. 8. Distribution of the warping harness.

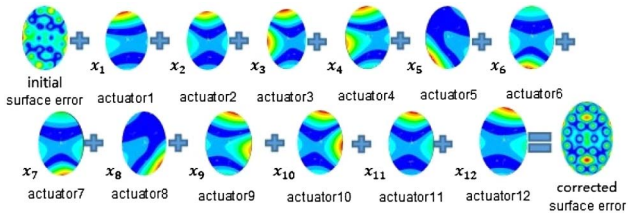

Fig. 9. Instruction of the calibration and simulation process.

$$ds_i^{\mathrm{Corr}} = ds_i + \sum_j x_j dx_{ji}, \tag{3}$$

where $d_{s_i}^{\mathrm{Corr}}$ is the corrected displacement of the ith node, ds_i is the uncorrected displacement of the ith node, x_j is the variable actuator input of the jth actuator, and $d_{x_{ji}}$ is the displacement of the ith node for the influence function of the jth actuator.

The actuator inputs are based on the minimum value of the surface mean square of the optical surface and represent the most correct result. The surface error formula is expressed as

$$E = \sum_{i=1}^{N} \omega_i \left(ds_i' - \sum_{j=1}^{M} A_j f_{ji} \right)^2. \tag{4}$$

In this expression, N is the number of nodes, ω_i is the weighting coefficient of node i, M is the number of actuator influence functions, ds_i is the surface deformation at node i, A_j is the actuator input of actuator influence function j, and f_{ji} is the surface deformation of actuator influence function j at node i. RMS denotes the RMS error function of mirror error E.

The deformation of each moment actuator is input as an optimization variable to minimize the RMS value of the optical surface. Each actuator correction force is calculated using the Sigfit adaptive control module. For an adjustable controlled mirror, the Sigfit software can calculate the actuator forces and displacements required to minimize the surface RMS and to correct any input deformation, including FE displacements or Zernike coefficients. Table 4 is the correction forces and moments, respectively, to correct the initial mirror-surface error, as shown in the left picture of Fig. 10.

Table 4. Results of the Actuator Correction

Actuator Number	Correction Force (N)	Correction Moment (N · mm)
1	−0.12943	−7.7658
2	0.40572	24.3432
3	0.65352	39.2112
4	−0.24742	−14.8452
5	−0.60841	−36.5046
6	−0.011633	−0.69798
7	0.12281	7.3686
8	−0.24679	−14.8074
9	−0.1376	−8.256
10	0.35826	21.4956
11	0.32357	19.4142
12	−0.29132	−17.4792

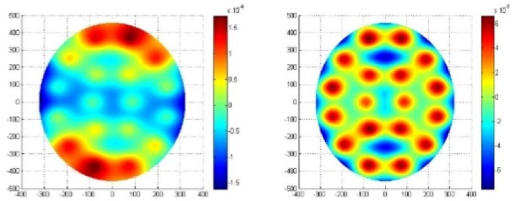

Fig. 10. Surface error distribution before and after correction.

The correction deformation phase maps both before and after application of the warping harness are shown in Fig. 10. The RMS value improves from 64.9 to 25.4 nm, and the improvement ratio of the RMS error is 37%.

The warping harness performance is specified in terms of the Zernike polynomial on the mirror surface mainly because it can very well fit the optical aberration and has good mathematical properties [14–16]. Therefore, the changes of values of each order of aberrations are the key index to evaluate warping harness performance. As listed in Table 5, different orders of aberrations before and after correction are obtained through the simulation process. The results show that both third- and fourth-order Zernike terms are found to be controllable.

As for the correction process of the tertiary mirror, the evaluation indicator is defined by TMT as plate scale distortion, which can be obtained from Eq. (5). The plate scale distortion represents the second- and third-order optical aberrations, which affect the mirror-surface quality directly. The evaluation process of the low-order surface error correction performance can be described as shown in Fig. 11. We substitute the results listed in Table 5 into Eq. (5) and then obtain the plate scale distortion values before and after correction, as expressed in Eq. (6):

$$\text{Plate Scale Distortion} = P = C_f \times |Z_4| + C_a \times \sqrt{Z_5^2 + Z_6^2}, \tag{5}$$

$$\begin{cases} P_1 = 3.69 \text{ mas} \\ P_2 = 0.053 \text{ mas}' \end{cases} \tag{6}$$

where $C_f = 44.45$ mas/μm RMS is static error, and $C_a = 63.7$ mas/μm RMS is dynamic error. P1 and P2 are the plate scale distortions before and after correction, respectively.

Table 5. Aberration Values Before and After Correction

Aberration	Polynomial	Term	Value (Before Correction)	Value (After Correction)
Piston	1	Z1	1	1
x-Tilt	$r\cos\theta$	Z2	−1.0383e-17	3.5077e-17
y-Tilt	$r\sin\theta$	Z3	−1.2542e-18	1.4165e-17
Focus	$2r^2 - 1$	Z4	6.5764e-07	−6.6625e-17
0° Astigmatism	$r^2\cos 2\theta$	Z5	4.8606e-05	1.8167e-07
45° Astigmatism	$r^2\sin 2\theta$	Z6	−3.6487e-05	6.6598e-07
x-Coma	$(3r^2 - 2)r\sin\theta$	Z7	2.7410e-07	−1.1849e-07
y-Coma	$(3r^2 - 2)r\cos\theta$	Z8	7.3762e-07	3.0121e-07

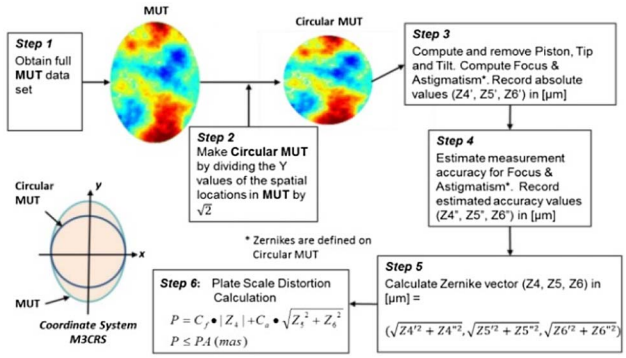

Fig. 11. Low-order surface error evaluation process of mirror under testing (MUT).

Table 6. Vectors of the Six Special Conditions

	X	X	Z
G1	−0.02	−0.71	−0.71
G2	−0.88	−0.17	−0.44
G3	−0.88	−0.39	−0.25
G4	−0.91	−0.30	−0.30
G5	−0.15	−0.73	−0.67
G6	−0.09	−0.64	−0.77

The design requirement is $P = 2$ mas. The result after the warping harness correction satisfies $P_2 \le P \le P_1$.

In addition, during the operation of the TMT tertiary mirror, there are six special conditions defined by the TMT, which represent six limiting situations affected by gravity. The mirror-surface error under six special conditions is analyzed. We define the six conditions as G1–G6, whose vector components of gravity along the X, Y, and Z axes are listed in Table 6, respectively.

We obtain the mirror-surface figure under the six conditions, as shown in Fig. 12, using the warping harness to obtain the deformation phase maps after the correction, as shown in Fig. 13. Table 7 lists the results of the mirror surface before and after correction under the six special conditions. From the results, we can see the correction ability of the warping harness.

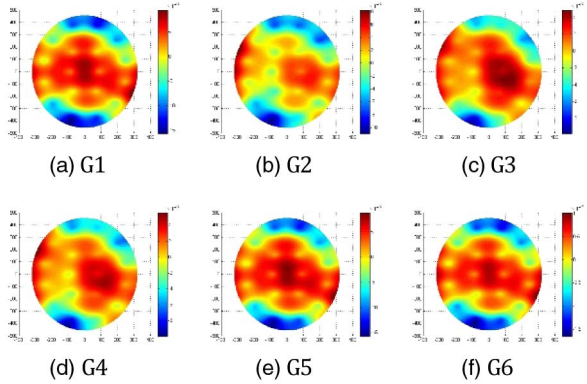

Fig. 12. Mirror-surface error under six special conditions.

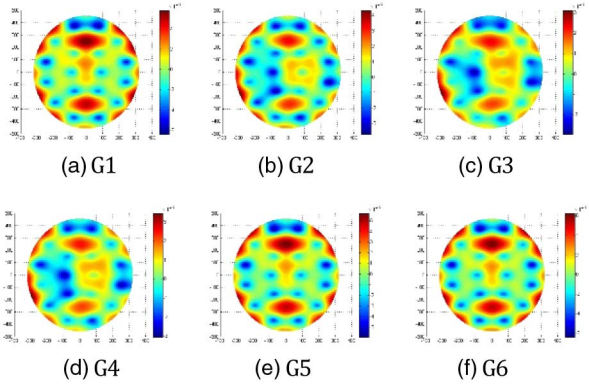

Fig. 13. Mirror-surface error under six special conditions after warping harness correction.

Table 7. Mirror Surface Before and After Correction Under Six Special Conditions

	Before Correction		After Correction	
Six Special Conditions	RMS (nm)	Slope RMS (μrad)	RMS (nm)	Slope RMS (μrad)
G1	57.1	0.804	20.7	0.696
G2	35.3	0.546	13.1	0.456
G3	28	0.388	10.5	0.291
G4	29.3	0.417	10.9	0.333
G5	55.4	0.77	19.9	0.661
G6	59.5	0.854	21.7	0.749

3. EXPERIMENT

Through theoretical calculation of the actuator moment of the warping harness, the design requirements of the corresponding displacement output stroke are obtained. Then, we develop the mechanical and electrical testing system with high-precision displacement–force–strain to assess the system errors. The design of the testing system is shown in Fig. 14, which includes the support plate, support cylindrical boss, eight support columns, two interface conversions, force actuators, and elastic blade.

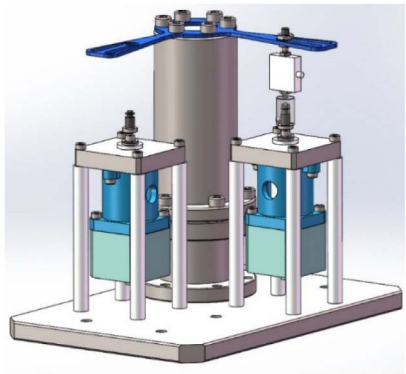

Fig. 14. Experimental structure design of the actuator test.

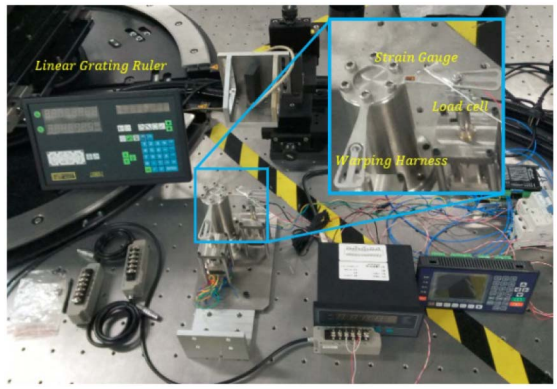

Fig. 15. Experimental platform construction.

The experimental platform construction is shown in Fig. 15, which includes the machine controller, grating scale, and load cell. The machine controller is used to control the stepping motor. The grating scale is used for displacement detection, and the load cell could detect the force magnitude.

A. Repeatability Test of the Displacement Output

The repeatability test is aimed to measure the displacement output precision and stability of the actuator, which is mainly affected by mechanical transmission error. During the testing process, the grating scale is used to measure the true displacement output value of the transmission shaft with the stepping motor rotating for one round. Repeat this measurement twenty times in two different periods of time and record the value of the displacements x_i, as shown in Fig. 16.

The repetitive error can be obtained with Eq. (7):

$$e_r = \sigma_{\bar{x}}/\bar{x} = \sqrt{\frac{\sum_{i=1}^{n}(x_i - \bar{x})^2}{n-1}}\Big/\bar{x} = 0.00256, \quad (7)$$

where e_r is the repetitive error, $\sigma_{\bar{x}}$ is standard deviation, $\bar{x}$ is the average value of the testing results, n is the sampling times, and the calculation result is 0.00256 mm, which is in a controllable range for the correction system.

B. Linearity and Zero-Returning Test

The linearity test is to see if the relationship between output displacement and motor rotation angle of the actuator is linear. It will be easier to control the output displacement for the actuator if the system has a good linear characteristic. The linearity measurement process used a machine controller that drove the stepping motor to run in a circle at the open-loop

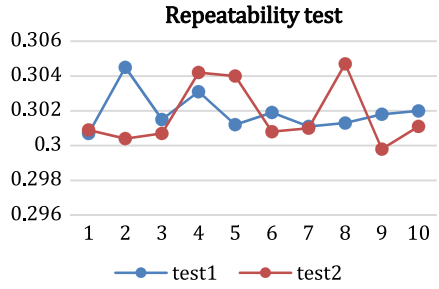

Fig. 16. Repeatability test of the displacement output.

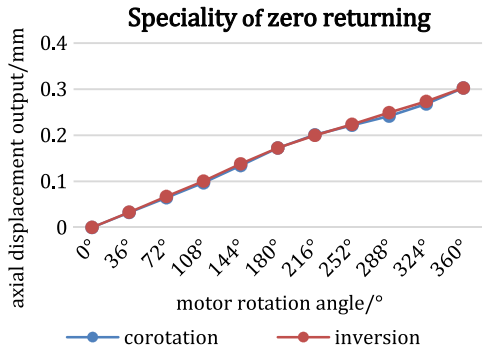

Fig. 17. Zero-returning test results.

speed, recording its displacement of 36° per interval. Therefore, we obtained a total of 10 displacement values. The linearity test result can be seen from the co-rotation curve in Fig. 17. The co-rotation curve shows that the displacement output is linear before 200° and a deviation after 200°, which may come from screw transmission error. Subsequently, in order to accomplish the zero-returning test, the motor was rerun in the reverse direction of the circle, and 10 displacement values at the same angle were recorded. The zero-returning test is aimed to assess whether the loading and unloading processes of the actuator are consistent with each other, which is mainly affected by the lost motion of the actuator. We drew the curve according to both the co-rotation and inversion test result, as shown in Fig. 17. The displacement output value of the inverted angle is basically consistent; thus, the lost motion of the actuator is small, which means the zero-returning property is good.

C. Stress Test of the Elastic Blade

The elastic blade generates elastic deformation because of the stepping motor output force, and the biggest stress occurs at the root of the blade. Through the FE simulation analysis, we can obtain the maximum stress of the elastic blade with the stepping motor making a turn equivalent to the output force, namely, 1.455 N, is 19.15 Mpa. To judge the accuracy of the FE simulation result, the strain gauge was bonded to the root of the blade to conduct the stress test. The other end of the strain gauge was connected to the strain regulator, as shown in Fig. 18. The stepping motor turn can cover the displacement output stroke of the correction. The stress test result

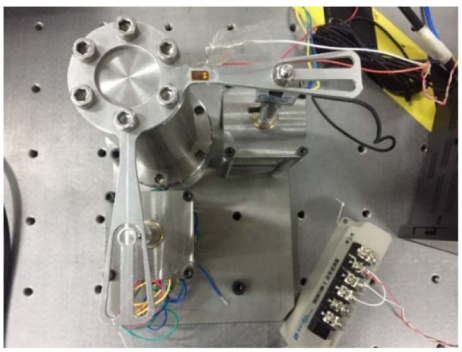

Fig. 18. Stress test of the elastic blade.

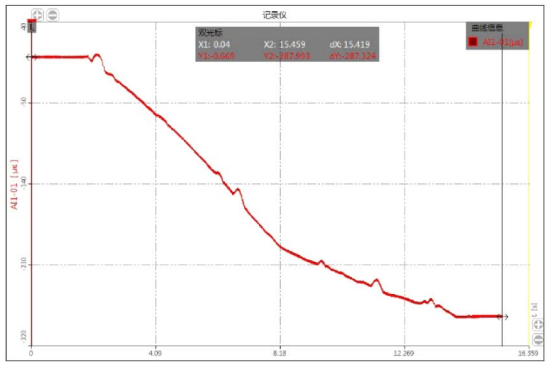

Fig. 19. Strain test curve of the elastic blade.

of the elastic blade is shown in Fig. 19. When the stepping motor was rotated at the maximum angle, the value of the strain was 2.87e-4 when the output force is 1.455 N. According to the formula $\sigma = E\varepsilon$, the stress was 20.58 Mpa.

The difference between the measured value and the simulation value is about 1.43 Mpa, which can be acceptable considering the equivalent error of output force. In addition, according to the test result, the safe factor is more than 24, since the ultimate yield strength of the elastic blade is 503 MPa, which proves the reliability of the structure.

5. CONCLUSIONS

We have designed a flexible moment actuator calibration system based on the requirements of the TMT tertiary mirror low-order aberrations. Structural FE and optimization design methods were used to optimize the blade thickness of the warping harness. The correction forces were calculated under the condition of gravity in the axial direction. The best results were achieved through linear superposition of the correction force and an RMS of 25.4 nm. The correction rate of the low-order defocus and astigmatism reached 99.8%. Subsequently, we built a mechanical and electrical testing system with high-precision displacement–force–strain to assess the system errors. Combined with the analysis and calculation results, the test of the warping harness correction component of the displacement, stress, strain-output precision, linearity, and repeatability was completed. The results can satisfy the requirement document of the TMT. This study has demonstrated that the warping harness plays an important role in the mirror-surface correction and low-order aberration removal. It verified the significance and value of the warping harness for large-aperture telescope correction technology and research in two aspects, namely, (1) instead of manually using a balance weight, the warping harness can correct low-order wavefront aberrations caused by unpredictable manufacturing errors and efficiently and conveniently support structure misalignment, and (2), more importantly, it can reduce the cost of mirror-surface processing, support system design, and installation.

Funding. National Natural Science Foundation of China (NSFC) (11503056).

Acknowledgment. The author is very grateful to Dr. Guo Peng and Dr. Zhao Hongchao for providing their valuable suggestions and help, and the TMT group for the use of their equipment and technology support.

REFERENCES

1. R. N. Wilson, F. Franza, P. Giordano, L. Noethe, and M. Tarenghi, "Active Optics," J. Mod. Opt. **3836**, 219–243 (1989).
2. B. Champigneulle and F. Pène, "Active optics correction forces for the VST 2.6-m primary mirror," Proc. SPIE **24**, 361–370 (2006).
3. T. S. Mast and J. E. Nelson, "Fabrication of large optical surfaces using a combination of polishing and mirror bending," Proc. SPIE **3**, 670–681 (1990).
4. G. Lemaître, "New procedure for making Schmidt corrector plates," Appl. Opt. **11**, 1630–1636 (1972).
5. E. Everhart, "Making corrector plates by Schmidt's vacuum method," Appl. Opt. **5**, 713–715 (1966).
6. J. Lubliner and J. E. Nelson, "Stressed mirror polishing. 1: a technique for producing nonaxisymmetric mirrors," Appl. Opt. **19**, 2332–2340 (1980).
7. J. E. Nelson and T. S. Mast, "Construction of the Keck observatory," Proc. SPIE **1236**, 47–55 (1990).
8. R. E. Parks, "Applications of stress polishing techniques as developed for the Keck observatory primary mirror fabrication," Proc. SPIE **1618**, 41–44 (1992).
9. L. Cavaller, J. Marrero, J. Castro, E. Morante, M. Ronquillo, and E. Hernández, "Design of the primary mirror segment support system for the E-ELT," Proc. SPIE **7012**, 70121F (2008).
10. F. Yang, H. C. Zhao, P. Guo, and Q. C. An, "Pre-construction of giant steerable science mirror for TMT," Proc. SPIE **9573**, 95730T (2015).
11. F. G. Wang, H. B. Yang, F. Yang, and X. X. Wu, "Optimization and analysis for the axis support points position of the large aperture mirror," Infrared Laser Eng. **36**, 877–880 (2007).
12. P. Guo, J. X. Zhang, F. Yang, and H. C. Zhao, "Optimization of TMT M3 prototype's support points," Laser Optoelectron. Prog. **52**, 198–203 (2015).
13. L. M. Zhang, B. Zhang, F. Yang, and M. Ming, "Design and test of force actuator in active optical system," Opt. Precis. Eng. **20**, 38–44 (2012).
14. V. N. Mahajan, "Zernike polynomials and wavefront fitting," in *Optical Shop Testing* (Wiley, 2006), pp. 498–546.
15. B. Qi, H. B. Chen, and N. L. Dong, "Wavefront fitting of interferograms with Zernike polynomials," Opt. Eng. **41**, 1565–1569 (2002).
16. R. J. Noll, "Zernike polynomials and atmospheric turbulence," J. Opt. Soc. Am. **66**, 207–211 (1976).